DJS Vol. 47(1) (2023) –pp.15-30 ISSN: 1012-5965

Delta Journal of Science
Available online at
https://djs.journals.ekb.eg/

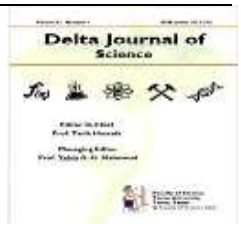

Research Article CHEMISTRY

Fluorescence superquenching of iodinated cyanine dyes using iron oxide nanoparticles in micellar media

Ali G. Al-Ayyat, Saleh A. Azim, Ibrahim A. Salem, El-Zeiny M. Ebeid(*) and Ehab A. Okba

Department of Chemistry, Faculty of Science, Tanta University, Tanta, Egypt

Corresponding author: Ehab A. Okba **e-mail :** ehab_okba@science.tanta.edu.eg

Received: 13/6/2023 **Accepted:** 24/7/2023

KEY WORDS

Theranostics, Iodinated cyanine dyes, Iron oxide nanoparticles, Fluorescence quenching, Micelles, Microwave synthesis.

ABSTRACT

Fluorescence quenching of iodinated cyanine dyes gained attention in recent years in the field of Theranostics whereby cyanine dyes loaded on FDA-approved feraheme form nanoprobes with quenched fluorescence. In the present paper, we report the fluorescence quenching of three iodinated cyanine dyes (I-III) using FDA-approved nano-iron oxide as potential candidates in the field of theranostics and other applications. The dyes were synthesized by solvent-free microwave technique. The electronic absorption, fluorescence spectra and excited state lifetimes were measured. Fluorescence quenching using iron oxide nanoparticles was studied in the presence and absence of SDS micelles. Micellar media enhance dynamic quenching at the expense of static quenching pathways as revealed by Stern-Volmer plots. The binding constants between the three iodinated cyanine dyes and iron oxide nanoparticles together with the second order quenching rate constants were calculated from Stern Volmer and modified Stern Volmer relations.

Fluorescence superquenching is a well-known phenomenon obtained when nanoparticles are applied as quenchers due to the remarkably low nanoparticle concentrations capable of causing efficient fluorescence quenching.

Introduction

For cyanine derivatives to be utilized in advanced applications, their photophysical properties are crucial. Occasionally, their absorption spectra extend into near-infrared (NIR) regions, ranging from 380 to 700 nm. The molar extinction coefficients are on the order of 10^4 M^{-1} cm^{-1} **(Jia et al., 2015)**. The Stokes shifts of substituted cyanine dyes in various polar solvents are commendable, making them more suitable than other known dyes for biological staining **(Ilina et al., 2019)**.

Photosensitizers, lasers, photodynamic therapy, semiconductors, and medical diagnosis by fluorescence sensing are just a few of the many applications of chemistry that make use of cyanine dyes **(Gopika et al., 2021)**. Cyanine dyes have good fluorescence quantum yields of aggregates and strong absorption in the visible region, making them promising candidates for the creation of optical devices **(Mishra et al., 2000)**.

Many cyanine dyes, including 1,1'-dioctadecyl-3,3,3' tetramethylindocarbo-cyanine perchlorate and 4,4'-difluoro-5,7-dimethyl-4-bora-3a,4a-diaza-s-indacene-3-propionic acid have been described as promising theranostic agents **(Reichel et al., 2019)**. To enhance their photophysical properties like photostability, photoconversion efficiency, singlet oxygen generation, and hyperthermia, cyanine nanoprobes like indocyanine Green (ICG), heptethine cyanine (IR780), and cypate were conjugated in polymeric micelles or inorganic nanoplatforms. Photodynamic therapy and photothermal therapy are supported by cyanines because of the excellent therapeutic benefits **(Bhattarai and Dai, 2017)**. As a multimodal contrast agent for MRI in humans, the theranostic Gd (DOTA)-cyanine dye has been developed and used with great effectiveness **(Wang et al., 2021)**.

The fluorescence quenching of cyanine derivatives using various quenchers like metal ions, carbon tetrachloride and acetone and has been studied by steady-state methods **(Tarazi et al., 2002; Biradar et al., 2007; Al-Kady et al., 2011a)**. The quenching of organic fluorophores by nanoparticles was reported **(Landes et al., 2001; Pramanik et al., 2007; Kotiaho et al., 2009)**, and both dynamic and static mechanisms are involved in the quenching process **(Huang and Murray, 2002, Ghosh et al., 2004, Lee and Suzuki, 2008)**. The quenching mechanism has significance in chemistry, biology, and medicine besides physics.

There are instances where the experimental data agree with the linear Stern-Volmer relationship, but there are also instances where the experimental results indicate a positive divergence from the linear Stern-Volmer plots **(Andre et al., 1979, Behera and Mishra, 1993)**. Multiple mechanisms, including singlet-to-triplet excitation, creation of charge transfer complexes in both ground and excited states, static and dynamic quenching, etc., have been proposed to account for this positive divergence.

High Stern-Volmer constants (in the range of 10^7-10^{11} M^{-1}) using metal nanoparticles are commonly associated with superquenching of organic dyes **(Morozov et al., 2020)**. Energy transfer between the dye molecules and the metal nanoparticles has been implicated as a cause of the fluorescence superquenching, along with the production of a nonfluorescent complex. The rate of collisional quenching of fluorescence from dyes like 3,7-diamino-2,8-dimethyl-5-phenyl phenazinium chloride by AgCl nanoparticles is affected by the size control of the AgCl nanoparticles in microemulsion media **(Pramanik et al., 2007)**.

Iron oxide nanoparticles are used in magnetic sealing, oscillation damping, position sensing, ultra-high density magnetic storage media, clinical diagnosis and therapy, biological labelling, tracking, imaging, detection, and separations **(Raj and Moskowitz 1990, Jordan et al., 2001, Bulte et al., 2002, Zeng et al., 2002).** Particle size, morphology of the particles, and size distribution all play a vital role in determining their features. Hematite is the most stable form of iron oxide, and it has numerous applications in science and technology.

Experimental

Materials and instruments

Fresh synthesized cyanine derivatives (I, II, and III) were produced according to established protocol **(Alganzory et al., 2017)**. Scheme 1 depicts the structures of the cyanine derivatives I, II, and III that were studied. Fluka supplied methanol and iron chloride ($FeCl_3$ 99%). Dodecyl sulphate (soda) from Sigma Aldrich. In all these experiments, double-distilled water was employed. A Shimadzu UV-160A Spectrophotometer was used to acquire the absorption spectra. A JASCO FP-8200 Spectrofluorometer was used to acquire emission spectra at a steady state condition. The picosecond fluorescence decay profiles were measured by single photon counting method using Fluor Hub (Horiba Scientific). Lifetime was

evaluated with software Fluo fit attached to the equipment.

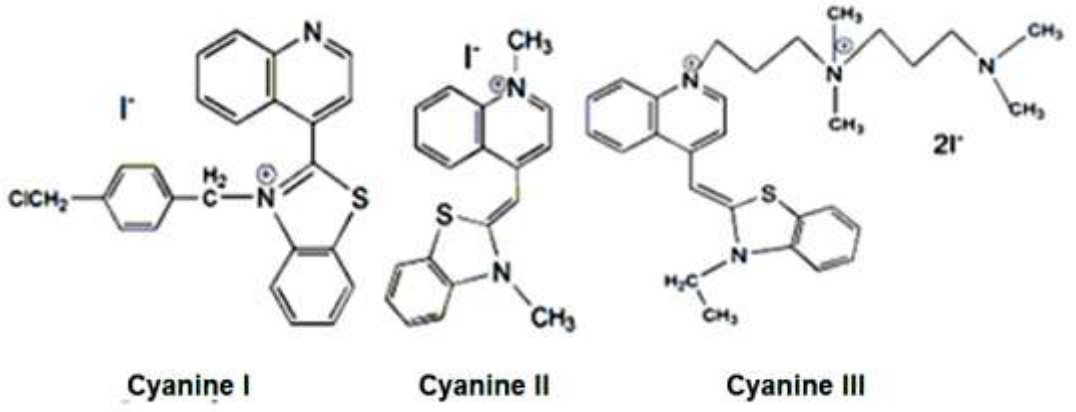

Scheme (1): The chemical structure of cyanine derivatives I, II and II

Synthesis of cyanine derivatives

Monomethine cyanine derivatives (I, II and III) were freshly synthesized using previously reported method **(Beilenson and Hamer, 1939)** as the follows:

Synthesis cyanine derivatives I and II

In the presence of triethylamine, monomethine cyanine dyes (I and II) were synthesized via the reaction of benzo thiazolium salts with 4-methylquinolinium salts. The yield is 80% and 87%, respectively, after 5 minutes of microwave irradiation at 320 W and 260 W of power [Scheme 2].

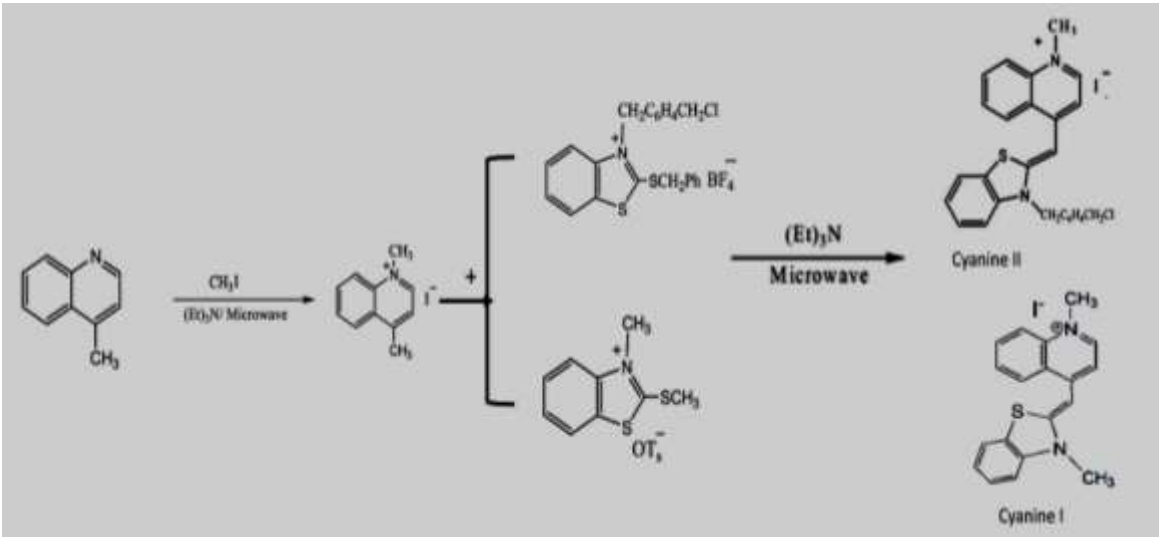

Scheme (2): Microwave synthesis of cyanine derivatives I and II

Synthesis cyanine derivative III

In the presence of dimethylformamide (DMF), equivalent amounts of monomethine cyanine dye A (1 mmol) and the corresponding diamino linker B (1 mmol) were mixed to produce

cyanine derivative III. After the addition of a few drops of triethylamine, the mixture was heated in a microwave for one hour and a half with 100 watts of power while being stirred continuously. TLC (eluent, petroleum ether: ethyl acetate, 3:1) was utilized to track the progression of the reaction. After being filtered out, the produced precipitate was washed with CH_2Cl_2 and then dried at 60 degrees Celsius.

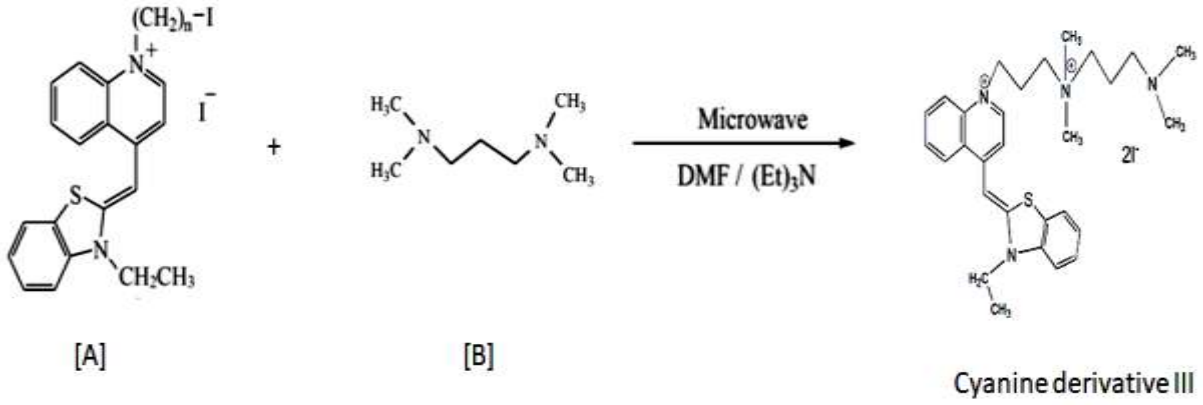

Scheme (3): Microwave synthesis of cyanine derivative III

Synthesis of iron oxide nanoparticles as a fluorescence quencher

A solution of 0.1 M $FeCl_3$ (15 ml) was added drop by drop to 100 ml of vigorously stirred boiling distilled water. The color changed from yellow ($FeCl_3$ solution) to red and upon excess addition of 0.1 M $FeCl_3$, the color turned to dark red. The resulting solution was heated to reflux and kept at that temperature for 30 min. The solution was then cooled to room temperature. Such colloidal solution can exist indefinitely without signs of precipitation. However, a reddish-brown precipitate was obtained upon dropping concentrated solution of sodium hydroxide **(Hamada and Matijević, 1981; Pu et al., 2006)**. The reaction mechanism was discussed **(Rufus et al., 2017)**. Boiling $FeCl_3$ in water produces purple-colored of hexa-aqua iron (III) complex ions ($[Fe(H_2O)_6]^{3+}$) **(Xiao et al., 2018)**. Aqua complex ions breakdown into deprotonated $[Fe(OH)(H_2O)]^{2+}$ species, which can be labelled FeIII-R.

Iron oxide nanoparticles quenched cyanin dye derivatives (I–III) fluorescence. 2 ml of 1×10^{-5}M cyanin dye derivatives in ethanol were combined with an appropriate volume of iron oxide nanoparticles solution as quencher.

Results and Discussion

UV–VIS electronic absorption spectrum of as prepared iron oxide nanoparticles is given in **Fig. (1)**

showing an absorption maximum at 385 nm in consistency with reported value **(Al-Kady et al., 2011b).** The band gap energy (E_{bg}) is calculated based on the maximum absorption band (385nm) of α-Fe_2O_3 nanoparticles as 3.22 eV according to following equation **(Rahman, 2011)**.

$$E_{bg} = \frac{1240}{\lambda}(eV)$$

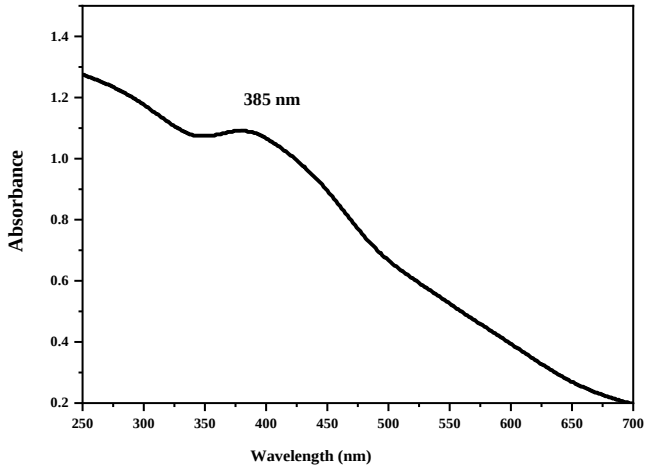

Fig. (1): Typical UV-Vis. spectrum of as-synthesized α-Fe_2O_3 nanoparticles in water

The electronic absorption and fluorescence spectra of cyanine derivatives (I-III)

The electronic absorption spectrum of 1 × 10^{-5} M ethanolic solutions show absorption peak maxima at 503 ,508 and 506 nm for cyanines I, II and III respectively (**Fig. 2**). These peaks are assigned to (π -π*) transition due to the resonance that occurs through the conjugated system between the tertiary and quaternary nitrogen atoms. The extensive conjugation leads to long-wavelength absorption maxima and high molar absorptivity. The fluorescence spectra ($\lambda_{ex.}$= 480 nm) show maximum fluorescence bands at 550, 563 and 563 nm for cyanines I, II and III respectively. Like other cyanines, the investigated cyanines are characterized by very small Stokes shifts (Table 1).

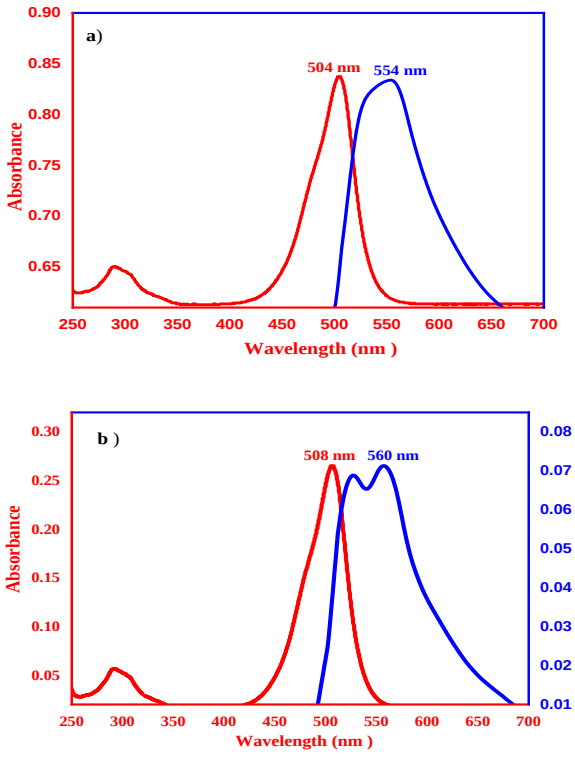

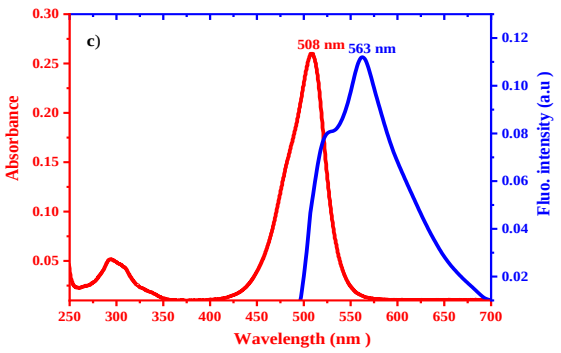

Fig. (2): Absorption and fluorescence spectra of cyanine dyes ethanolic solutions (a) cyanine I, (b) cyanine II and (c) cyanine III

Effect of solvent polarity on the absorption and emission spectra of cyanines I, II and III

The absorption spectra of derivatives I, II and III are shown in **Fig. (3-5)**. The molar extinction coefficients $\varepsilon_{max.}$ and maximum wavelengths ($\lambda_{max.)}$ are given in Table (1). The emission spectra of cyanine I, as a model in different solvents is shown in **Fig. (6).**

Table (1): Spectral maxima and photo physical parameters of cyanine derivatives (I) in different solvent

Solvent	$\lambda_{max.}$ (Abs.) (nm)	ε_{max} $M^{-1}cm^{-1}$	$\lambda_{max.}$ (Em.) (nm)	$\Delta\bar{\nu}$ cm^{-1}	E_T^N	$E_T(30)$ kcal/mol	Δf	Dielectric constant(ε)	Dipole moment(μ)
Acetone	504	97800	557	1887.9	0.355	42.2	5.1	21.3	2.87
Acetonitrile	503	93200	550	1698.8	0.461	45.6	5.8	37.5	3.85
Dioxane	505	75400	560	1944.8	0.164	36.1	4.8	2.25	0.45
DMF	506	89900	555	1744.8	0.386	43.8	6.4	36.7	3.86
DMSO	509	79600	558	1725.2	0.444	45.0	7.2	46.7	3.92
n-Butanol	507	97100	557	1770.5	0.586	50.2	3.9	17.8	1.66
Water	503	60700	566	2212.8	1.0	63.1	10.2	80.1	1.82
Methanol	504	93200	554	1790.7	0.762	55.4	5.1	32.7	1.72
Isopropanol	505	71400	561	1976.6	0.546	49.2	3.9	17.9	1.66
n-propanol	505	89900	556	1816.3	0.617	48.6	4.0	20.1	1.68

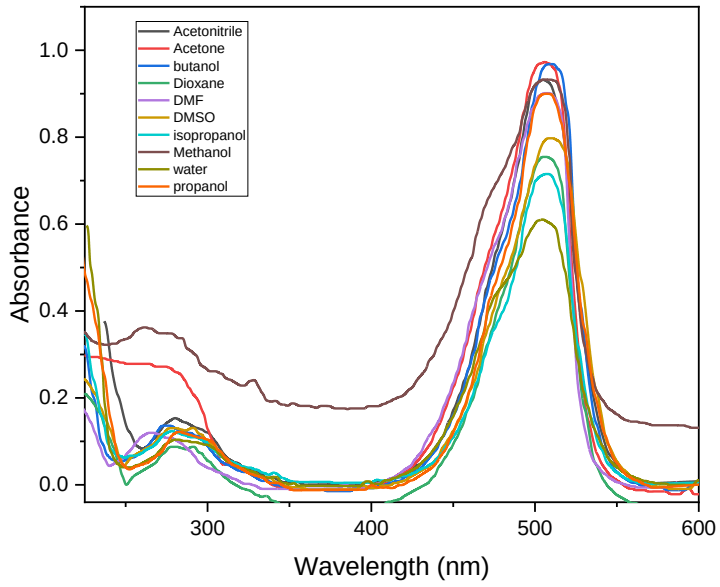

Fig. (3): Absorption spectra of 1×10^{-5} M cyanine I in different solvents

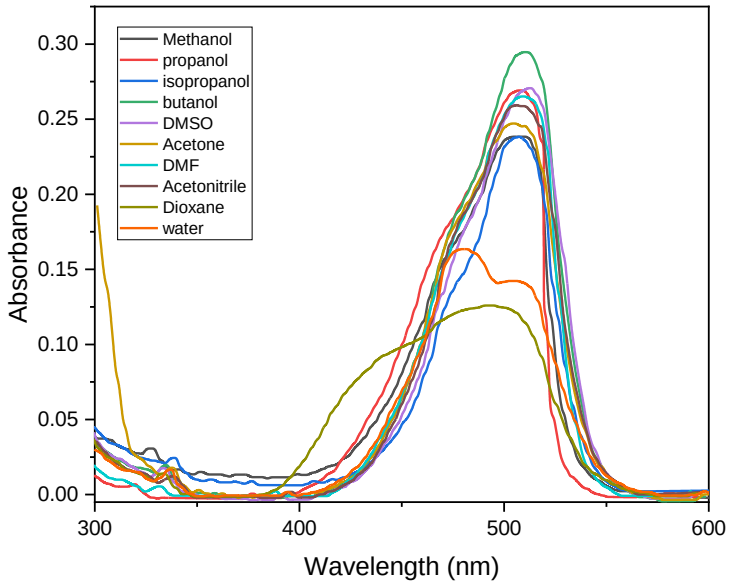

Fig. (4): Absorption spectra of 1×10^{-5} M cyanine II in different solvents

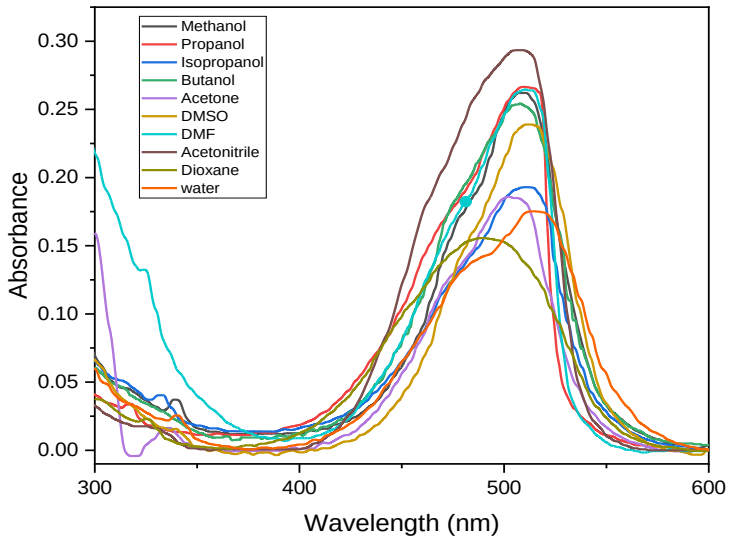

Fig. (5): Absorption spectra of 1×10^{-5} M cyanine III in different solvents

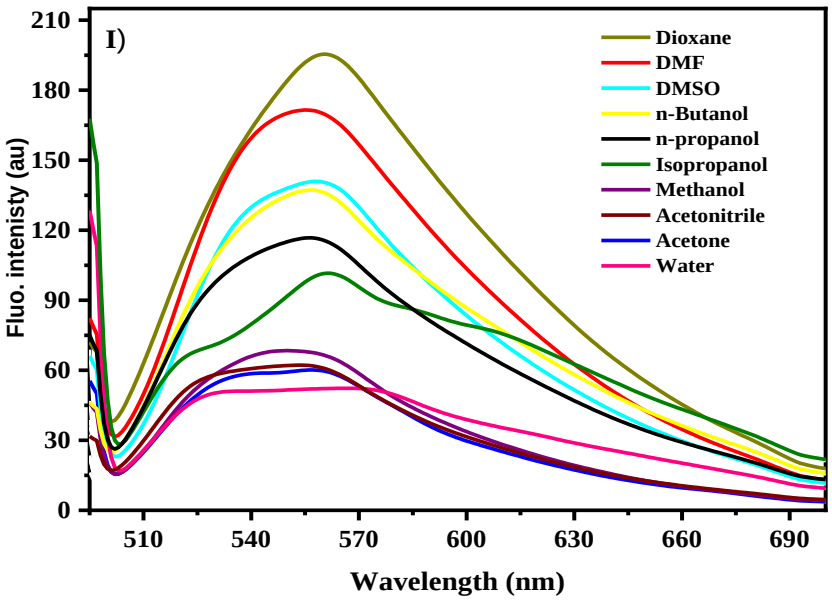

Fig. (6): Fluorescence spectra ($\lambda_{ex.}$= 480) of 1×10^{-5} M cyanine I in different solvents

Fluorescence quenching of cyanines I, II and III using iron oxide nanoparticles.

The fluorescence quenching of cyanines I-III using iron oxide nanoparticles as a quencher reveals no spectral pattern change and no other emission bands were noticed revealing the absence of emissive exciplex under applied experimental conditions.

The Stern-Volmer equation (1) was applied to study the fluorescence quenching behavior **(Lakowicz, 2013)**.

$$\frac{I_0}{I} = 1 + K_{SV}[Q] \ldots \quad (1)$$

where I_0 and I are the fluorescence intensities in the absence and presence of quencher, respectively, K_{SV} is the Stern–Volmer quenching constant and [Q] is the quencher concentration. The Stern–Volmer plots are nonlinear with positive deviation as shown in **Fig. (7)**. Similar experimental results were reported by others **(Tablet and Hillebrand, 2007; Melavanki et al., 2008; Evale and Hanagodimath, 2009; Melavanki et al., 2009; Evale and Hanagodimath, 2010)**. The positive deviation from linearity suggests that the quenching is not purely dynamic but is due to the simultaneous dynamic and static quenching types.

The fluorescence quenching of cyanines I-III using iron oxide nanoparticles was further studied in presence SDS micelles (2×10^{-3} M) showing linear Stern-Volmer plots with correlation coefficient of 0.995 as shown in **Fig. (7)**. This indicates a dominant dynamic quenching mechanism in the presence of SDS micelles.

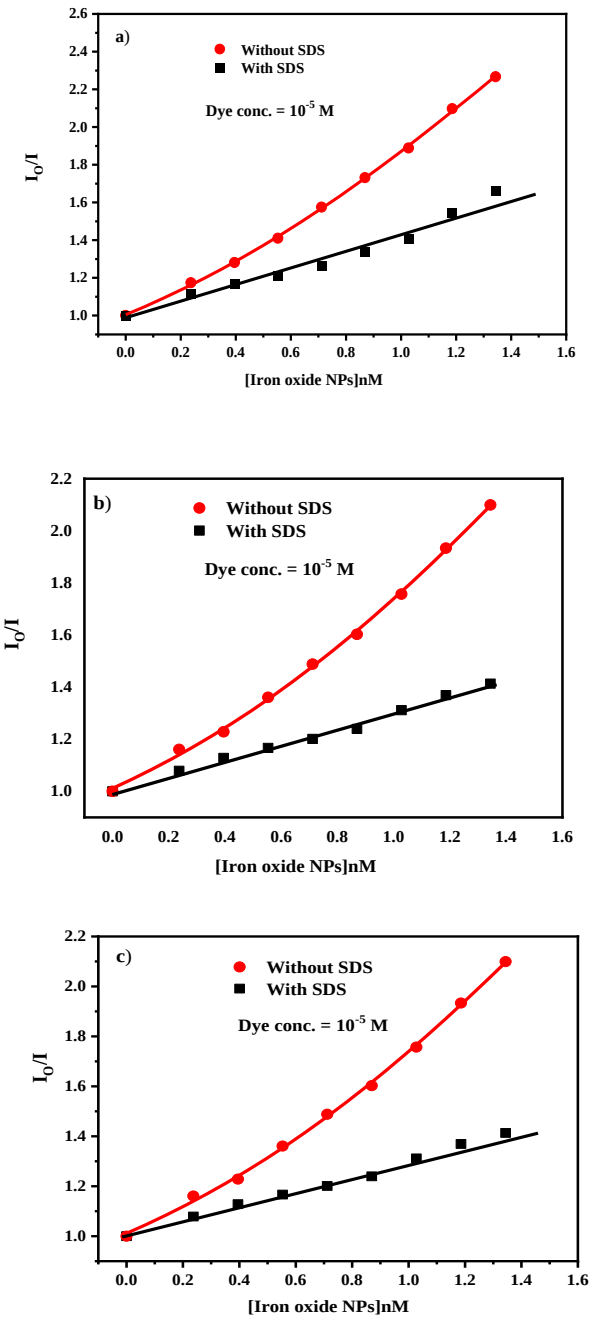

Fig. (7): Stern-Volmer plots for the fluorescence quenching of cyanines (a) I, (b) II, and (c) III using iron oxide nanoparticles as a quencher in the presence and absence of 2×10^{-2} M SDS.

Calculation of Binding constants

For non-linear Stern-Volmer plots obtained in non-micellar media, the extended Stern Volmer equation (2) was applied **(Lakowicz, 2006)**:

$$\frac{\left[\frac{I_0}{I}\right]-1]}{[Q]} = (K_{SV} + K_g) + (K_{SV}K_g)[Q] \ldots\ldots\ldots (2)$$

where K_{SV} and Kg are the dynamic Stern-Volmer quenching and ground-state binding constants of the complex between cyanine dyes and iron oxide nanoparticles. Upon fitting experimental data to Eq. (2) two quenching behaviors are recognized with the quenching at higher quencher concentrations assigned to dominant static quenching for which both K_{SV} and Kg have been determined. **Fig. (8)** shows plots of $[I_0/I - 1]/[Q]$ versus [Q]. Table 2 shows the K_{SV} and Kg values obtained from intercepts and slopes of the second stage. The obtained dynamic quenching K_{SV} constants have nearly the same values obtained for the dynamic quenching plots according to Eq. (1).

The excited state lifetimes τ values of cyanines I, II and III were measured as 5.46, 5.18 and 4.71 ns for cyanines I, II and III respectively. From the lifetimes and K_{SV} values, the second order quenching rate constants k_q were determined according to the relation: $k_q = K_{sv}/\tau$ and the values are given in Table 1 with k_q^a in SDS micelles being of higher values compared with k_q^b values in non-micellar media.

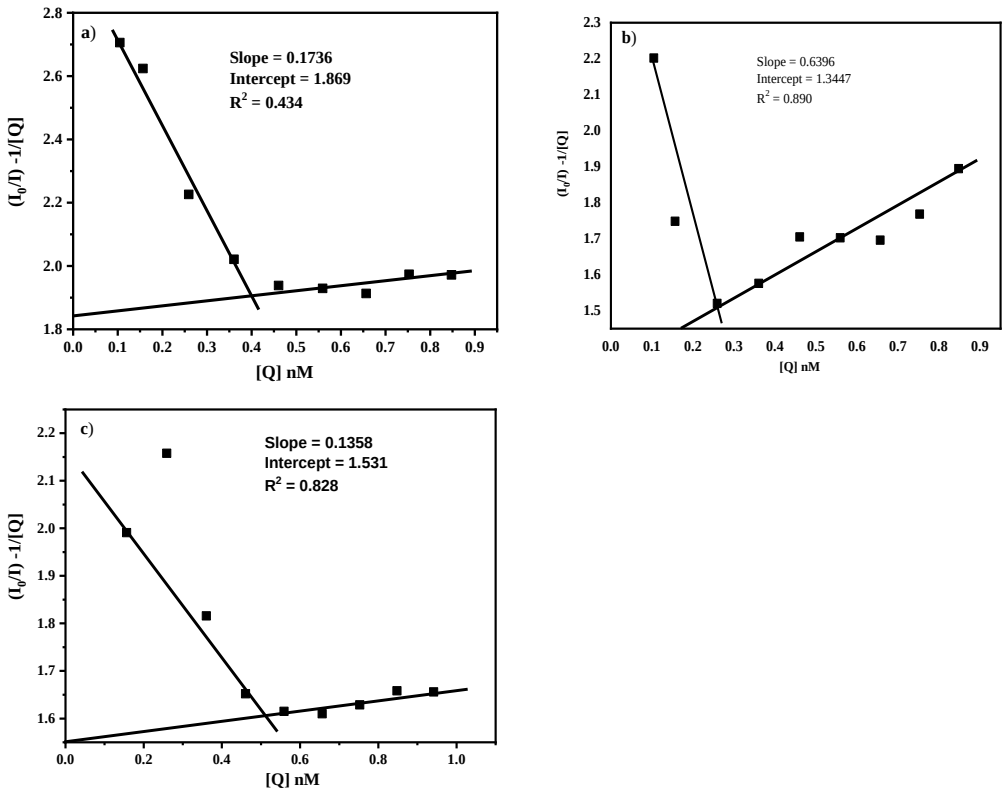

Fig. (8): Plots of $[I_0 /I - 1]/[Q]$ versus [Q] for Cyanines I–III in absence of SDS solutions

Table (2): Quenching parameters of cyanines I–III using iron oxide nanoparticles as a quencher in the presence SDS solution.

Cyanine	$K_{sv}^{a} \times 10^{8}(M^{-1})$	$K_{sv}^{b} \times 10^{8}(M^{-1})$	$K_{sv}^{c} \times 10^{8}(M^{-1})$	$K_{g}^{a} \times 10^{8}(M^{-1})$	τ (ns)	k_{q}^{a} $(M^{-1}s^{-1})$	k_{q}^{b} $(M^{-1}s^{-1})$
I	11.35	10.90	7.67	15.92	5.46	20.78	19.96
II	12.62	7.79	11.68	8.20	5.18	24.36	15.03
III	11.41	10.07	4.96	13.48	4.71	24.22	21.38

Ksv $^{(a)}$: From eq. 1 in absence of micelles (SDS).
Ksv $^{(b)}$: From eq. 2.
Ksv $^{(c)}$: In presence of SDS micelles
Kg: Binding constant.
kq^{a}: The second order quenching rate constant from equation 1
kq^{b}: The second order quenching rate constant from equation 2
τ_0 (ns): Excited state lifetime.

Conclusion

In this study, electronic absorption and emission spectra of three iodinated cyanine dyes were studied in different solvents. Superquenching of the cyanine dyes fluorescence was conducted by iron oxide nanoparticles giving high Stern-Volmer constants values in range of 10^{8} M^{-1}. The quenching of cyanines (I-III) with iron oxide nanoparticles is due to dynamic and static quenching. The quenching process in presence of SDS micelle is mainly dynamic quenching indicating the efficiency of micelle in inhibition of static quenching due to solubilization effect. As a result of the remarkably high quenching of cyanines fluorescence by iron oxide nanoparticles, it is possible to use cyanines- iron oxide nanoparticles system as nanoprobes in theranostics whereby cyanine dyes fluorescence is regenerated upon liberation from iron oxide nanoparticles.

Author Contributions

Ali G. Al-Ayyat: Conceptualization, Investigation, Methodology, Visualization, Validation, Writing original draft. **Saleh A. Azim**: Supervision. **Ibrahim A. Salem**: Supervision. **El-Zeiny M. Ebeid:** Conceptualization, Investigation, Methodology, Visualization, Validation, Writing - Reviewing and Editing, Supervision. **Ehab A. Okba**: Visualization, investigation, manuscript preparation, Reviewing and Editing.

Data Availability

All data generated or analyzed during this study are included in this published article.

Declarations

Ethical Approval

This article does not contain any studies involving animals performed by any of the authors.

Consent to Participate

This article does not contain any studies involving animals performed by any of the authors.

Consent to Publish

All authors mentioned in the manuscript have given consent for submission and subsequent publication of the manuscript.

Conflict of Interest

The authors have declared no conflict of interest.

References

Al-Kady, A. S., M. Gaber, M. M. Hussein, and E.-Z. M. Ebeid. 2011a. Structural and fluorescence quenching characterization of hematite nanoparticles. *Spectrochim Acta. Mol. Biomol. Spectros*., 83: 398-405.

Al-Kady, A. S., M. Gaber, M. M. Hussein, E.-Z. M. J. S. A. P. A. M. Ebeid 2011b. Structural and fluorescence quenching characterization of hematite nanoparticles. *Spectrochim Acta. Mol. Biomol. Spectros*., 83: 398-405.

Alganzory, H. H., W. A. El-Sayed, M. H. Arief, M. S. Amine, and E.-Z. M. Ebeid. 2017. Microwave synthesis and fluorescence properties of homo- and heterodimeric monomethine cyanine dyes TOTO and their precursors. *Green Chem. Lett. Rev.*, 10: 10-22.

Andre, J., L. Vincent, D. O'Connor, and W. Ware. 1979. Applications of fast Fourier transform to deconvolution in single photon counting. *J. Phys. Chem.*, 83: 2285-2294.

Behera, P. K., and A. K. Mishra. 1993. Static and dynamic model for 1-naphthol fluorescence quenching by carbon tetrachloride in dioxane—acetonitrile mixtures. *J. Photochem. Photobiol. Chem..*, 71: 115-118.

Beilenson, B., and F. M. Hamer. 1939. 34. Preparation of simple cyanines. *J. Chem. Soc*. (Resumed): 143-151.

Bhattarai, P., and Z. Dai. 2017. Cyanine based nanoprobes for cancer theranostics. Advanced healthcare materials 6: 1700262.

Biradar, D., J. Thipperudrappa, and S. Hanagodimath. 2007. Fluorescence quenching studies of 1, 3-diphenyl benzene. *Spectros Lett.*, 40: 559-571.

Bulte, J. W., I. D. Duncan, and J. A. Frank. 2002. In vivo magnetic resonance tracking of magnetically labeled cells after transplantation. *J Cerebr Blood Flow Metabol.*, 22: 899-907.

Evale, B. G., and S. Hanagodimath. 2009. Fluorescence quenching of newly synthesized biologically active coumarin derivative by aniline in binary solvent mixtures. *J. Lumin.*, 129: 1174-1180.

Evale, B. G., and S. Hanagodimath. 2010. Static and dynamic quenching of biologically active coumarin derivative by aniline in benzene–acetonitrile mixtures. *J. Lumin.*, 130: 1330-1337.

Ghosh, S. K., A. Pal, S. Kundu, S. Nath, and T. Pal. 2004. Fluorescence quenching of 1-methylaminopyrene near gold nanoparticles: size regime dependence of the small metallic particles. *Chem. Phys. Lett*., 395: 366-372.

Gopika, G., P. H. Prasad, A. Lekshmi, S. Lekshmypriya, S. Sreesaila, C. Arunima, M. S. Kumar, A. Anil, A. Sreekumar, and Z. S. Pillai. 2021. Chemistry of cyanine dyes-A review. Materials Today: *Proceedings*, 46: 3102-3108.

Hamada, S., and E. Matijević. 1981. Ferric hydrous oxide sols. IV. Preparation of uniform cubic hematite particles by hydrolysis of ferric chloride in alcohol—water solutions. *J. Colloid Interface Sci.*, 84: 274-277.

Huang, T., and R. W. Murray. 2002. Quenching of [Ru (bpy) 3] 2+ fluorescence by binding to Au nanoparticles. *Langmuir*, 18: 7077-7081.

Ilina, K., W. M. MacCuaig, M. Laramie, J. N. Jeouty, L. R. McNally, and M. Henary. 2019. Squaraine dyes: molecular design for different applications and remaining challenges. *Bioconjugate chem*., 31: 194-213

Jia, H., Y. Lv, S. Wang, D. Sun, and L. Wang. 2015. Synthesis, crystal structures, and spectral properties of double N-alkylated dimethine cyanine dyes and their interactions with biomolecules and living cells. *RSC advances*, 5: 4681-4692.

Jordan, A., R. Scholz, K. Maier-Hauff, M. Johannsen, P. Wust, J. Nadobny, H. Schirra, H. Schmidt, S. Deger, and S. Loening. 2001. Presentation of a new magnetic field therapy system for the treatment of human solid tumors with magnetic fluid hyperthermia. *J. Magn. Magn. Mater*, 225: 118-126.

Kotiaho, A., R. Lahtinen, H.-K. Latvala, A. Efimov, N. V. Tkachenko, and H. Lemmetyinen. 2009. Effect of gold nanoparticles on intramolecular exciplex emission in organized porphyrin–fullerene dyad films. *Chem. Phys. Lett.*, 471: 269-275.

Lakowicz, J. R. 2006. Principles of fluorescence spectroscopy, Springer.

Lakowicz, J. R. 2013. Principles of fluorescence spectroscopy, Springer science & business media.

Landes, C. F., M. Braun, and M. A. El-Sayed. 2001. On the nanoparticle to molecular size transition: fluorescence quenching studies. *J. Phys. Chem. B* ., 105: 10554-10558.

Lee, I.-Y. S., and H. Suzuki. 2008. Quenching dynamics promoted by silver nanoparticles. *J. Photochem. Photobiol. Chem*., 195: 254-260.

Melavanki, R., R. Kusanur, M. Kulakarni, and J. Kadadevarmath. 2008. Role of solvent polarity on the fluorescence quenching of newly synthesized 7, 8-benzo-4-azidomethyl coumarin by aniline in benzene–acetonitrile mixtures. *J. Lumin*., 128: 573-577.

Melavanki, R., R. Kusanur, J. Kadadevaramath, and M. Kulakarni. 2009. Quenching mechanisms of 5BAMC by aniline in different solvents using Stern–Volmer plots. *J. Lumin*., 129: 1298-1303.

Mishra, A., R. K. Behera, P. K. Behera, B. K. Mishra, and G. B. Behera. 2000. Cyanines during the 1990s: a review. *Chem Rev*., 100: 1973-2012.

Morozov, V. N., M. A. Kolyvanova, O. V. Dement'eva, V. M. Rudoy, and V. A. Kuzmin. 2020. Fluorescence

superquenching of SYBR Green I in crowded DNA by gold nanoparticles. *J.Lumin*., 219: 116898.

Pramanik, S., S. C. Bhattacharya, and T. Imae. 2007. Fluorescence quenching of 3, 7-diamino-2, 8-dimethyl-5-phenyl phenazinium chloride by AgCl and Ag nanoparticles. *J Lumin*., 126: 155-159.

Pu, Z., M. Cao, J. Yang, K. Huang, and C. Hu. 2006. Controlled synthesis and growth mechanism of hematite nanorhombohedra, nanorods and nanocubes. *Nanotechnol.*, 17: 799.

Rahman, M. M., Sher Bahadar Khan. 2011. Nanomaterials, pp. 327. *In* T. Greblo [ed.]. intech; janeza Trdine 9, 51000 Rijeka, Croatia, intechopen.com.

Raj, K., and R. Moskowitz. 1990. Commercial applications of ferrofluids. *J. Magn. Magn. Mater*., 85: 233-245.

Reichel, D., M. Tripathi, P. Butte, R. Saouaf, and J. M. Perez. 2019. Tumor-Activatable Clinical Nanoprobe for Cancer Imaging. Nanotheranostics 3: 196-211.

Rufus, A., N. Sreeju, V. Vilas, and D. Philip. 2017. Biosynthesis of hematite (α-Fe2O3) nanostructures: size effects on applications in thermal conductivity, catalysis, and antibacterial activity. *J. Mol. Liq*., 242: 537-549.

Tablet, C., and M. Hillebrand. 2007. Quenching of the fluorescence of 3-carboxy-5, 6-benzocoumarin by aromatic amines. *J. Photochem. Photobiol. Chem.*, 189: 73-79.

Tarazi, L., H. Choi, J. C. Mason, J. Sowell, L. Strekowski, and G. Patonay. 2002. Characterization of a novel crown ether-bearing near-infrared heptamethine cyanine dye. A study of fluorescence quenching by lithium. *Microchem. J.*, 72: 55-62.

Wang, X., H. N. Chan, N. Desbois, C. P. Gros, F. Bolze, Y. Li, H. W. Li, and M. S. Wong. 2021. Multimodal Theranostic Cyanine-Conjugated Gadolinium (III) Complex for In Vivo Imaging of Amyloid-β in an Alzheimer's Disease Mouse Model. ACS Applied Materials & Interfaces 13: 18525-18532.

Xiao, N., J. X. Dong, S. G. Liu, N. Li, Y. Z. Fan, Y. J. Ju, N. B. Li, and H. Q. Luo. 2018. Multifunctional fluorescent sensors for independent detection of multiple metal ions based on Ag nanoclusters. Sensors and Actuators B: Chemical 264: 184-192.

Zeng, H., J. Li, J. P. Liu, Z. L. Wang, and S. Sun. 2002. Exchange-coupled nanocomposite magnets by nanoparticle self-assembly. *Nat*. 420: 395-398.

الانخفاض الفائق في شده الانبعاث الفلوريسيني لبعض صبغات السيانين المعالجة باليود باستخدام جسيمات أكسيد الحديد النانوية و الميسلات

علي جمال العياط ، أ.د/ صالح عبد العظيم ، أ.د/ ابراهيم سالم ، أ.د/الزيني موسي عبيد، د/ ايهاب عبد القوي

قسم الكيمياء - كلية العلوم- جامعة طنطا

اكتسبت ظاهره الانبعاث الفلوريسيني لصبغات السيانين اهتمامًا كبيرا في السنوات الأخيرة في مجال تشخيص وعلاج الامراض، حيث يتم تحميل أصباغ السيانين على مواد نانويه مصرح بها من إدارة الأغذية والعقاقيرFDA. في هذا البحث تم دراسة تثبيط الانبعاث الفلوريسيني لثلاثة أصباغ من السيانين باستخدام أكسيد الحديد النانوي المصرح به من إدارة الأغذية والعقاقير (FDA) كاحد اهم المواد المستخدمة في مجال العلاج الكيميائي والتطبيقات الأخرى ، حيث تم تحضير اصباغ السيانين باستخدام تقنية الميكروويف باستخدام الحد الأدنى من المذيبات. كما تم قياس أطياف الامتصاص والانبعاث الفلورسيني و كذلك فترات الحياة للحالة المثارة في المذيبات المختلفة. دراسة ظاهره تثبيط الفلورسينس لاصباغ السيانين باستخدام جزيئات أكسيد الحديد النانوية قد تمت في وجود وفي غياب المواد ذات النشاط السطحي مثل SDS وقد اتضح ان وجود الميسلات تعمل على زيادة التثبيط الفلوريسيني بطريقه ديناميكيه على حساب التثبيط الفلوريسني الاستاتيكى. ايضا تم حساب ثوابت الارتباط بين أصباغ السيانين الثلاثة وجسيمات أكسيد الحديد النانوية وحساب ثوابت معدلات التثبيط الفلوريسيني من الدرجة الثانية من علاقات شتيرن فولمر وعلاقات شتيرن فولمر المعدلة .الانخفاض الفائق في شده الانبعاث الفلوريسسني هو ظاهرة معروفة عند استخدام الجسيمات النانوية كعوامل تثبيط للانبعاث الفلوريسيني بسبب تركيزات الجسيمات النانوية المنخفضة والقادرة على علي التثبيط الفائق للانبعاث الفلوريسيني وبالتالي يمكن استخدام هذه الظاهره في التعيين الكمي لهذه الجسيمات.